# Adaptive significance of age- and light-related variation in needle structure, photochemistry, and pigments in evergreen coniferous trees

**James Oluborode**
University of Life Sciences in Poznań
**Tamara Chadzinikolau**
University of Life Sciences in Poznań
**Magda Formela-Luboińska**
University of Life Sciences in Poznań
**Zi-Piao Ye**
Jinggangshan University
**Piotr Robakowski**
piotr.robakowski@up.poznan.pl
University of Life Sciences in Poznań

**Research Article**

**Keywords:** adaptation to light, chlorophyll a fluorescence, leaf age, photosynthesis, photosynthetic pigments

**Posted Date:** July 19th, 2024

**DOI:** https://doi.org/10.21203/rs.3.rs-4648348/v1



**Additional Declarations:** No competing interests reported.

**Version of Record:** A version of this preprint was published at Photosynthesis Research on December 20th, 2024. See the published version at https://doi.org/10.1007/s11120-024-01125-2.

# Adaptive significance of age- and light-related variation in needle structure, photochemistry, and pigments in evergreen coniferous trees

James Oluborode[1], Tamara Chadzinikolau[2], Magda Formela-Luboińska[2], Zi-Piao Ye[3], Piotr Robakowski[1*]

[1]Faculty of Forestry and Wood Technology, Poznan University of Life Sciences, Wojska Polskiego 71E, 60-625 Poznań, Poland, phone: +48618487738, e-mail: oluborodejames@gmail.com, piotr.robakowski@up.poznan.pl;

[2]Faculty of Agriculture, Horticulture and Bioengineering, Poznan University of Life Sciences; Wołyńska 35, 60-637 Poznań, Poland, phone: +48618466038, e-mail: tamara.chadzinikolau@up.poznan.pl, magda.formela-luboinska@up.poznan.pl;

[3]School of Life Sciences, Jinggangshan University, Ji'an, 343009, China, e-mail: yezp@jgsu.edu.cn

[*]Author for correspondence: piotr.robakowski@up.poznan.pl

ORCID:
JO https://orcid.org/0000-0002-8537-4639
TCh https://orcid.org/0000-0001-8283-8779
MF-L https://orcid.org/0000-0003-4341-5399
Z-PY https://orcid.org/0000-0002-7598-1822
PR https://orcid.org/0000-0001-5564-7360

## Abstract

Evergreen conifers thrive in challenging environments by maintaining multiple sets of needles, optimizing photosynthesis even under harsh conditions. This study aimed to investigate the relationships between needle structure, photosynthetic parameters, and age along the light gradient in the crowns of *Abies alba*, *Taxus baccata*, and *Picea abies*. We hypothesized that: (1) Needle structure, photochemical parameters, and photosynthetic pigment content would correlate with needle age and light levels in tree crowns. (2) The photosynthetic capacity of ageing needles would decline and adjust to the increasing self-shading of branches. Our results revealed a non-linear increase in the leaf mass-to-area ratio. The maximum quantum yield of photosystem II photochemistry decreased linearly with needle age without reaching levels indicative of photoinhibition. Decreased maximum electron transport rates ($ETR_{max}$) were linked to declining values of saturation photosynthetic photon flux and increasing non-photochemical quenching of fluorescence (*NPQ*), indicating energy losses as heat. The chlorophyll *a* to chlorophyll *b* ratio linearly decreased, suggesting older needles sustain high light capture efficiency. These findings offer new insights into the combined effects of needle ageing and self-shading on photochemistry and pigment content. This functional needle balance highlights the trade-off between the costs of long-term needle retention and the benefits of efficient resource utilization. In environments where air temperature is less of a constraint on photosynthesis due to climate warming, evergreen coniferous trees could sustain or enhance their photosynthetic capacity. They can achieve this by shortening needle lifespan and retaining fewer cohorts of needles with higher $ETR_{max}$ and lower *NPQ* compared to older needles.

**Keywords**: adaptation to light, chlorophyll *a* fluorescence, leaf age, photosynthesis, photosynthetic pigments

***List of abbreviation***

| Abbreviation | Definition | Units |
|---|---|---|
| *Car* | Total needle carotenoid concentration | mg $g^{-1}$ |
| *Car* | Total needle carotenoid content | g $m^{-2}$ |
| $Chl_{tot}$ | Total needle chlorohyll concentration | mg $g^{-1}$ |
| $Chl_{tot}$ | Total needle chlorophyll content | g $m^{-2}$ |
| $Chl_a$ | Chlorophyll *a* concentration | mg $g^{-1}$ |
| $Chl_a$ | Chlorophyll *a* content | g $m^{-2}$ |
| $Chl_b$ | Chlorophyll *b* concentration | mg $g^{-1}$ |
| $Chl_b$ | Chlorophyll *b* content | g $m^{-2}$ |
| $F_v/F_m$ | Maximum quantum yield of PSII photochemistry | dimensionless |
| $ETR_{max}$ | Apparent maximum electron transport rate (*ETR*) | µmol $m^{-2}$ $s^{-1}$ |
| *LMA* | Leaf mass-to-area ratio | g $m^{-2}$ |
| *NPQ* | Non-photochemical quenching of fluorescence | dimensionless |
| $PPF_{sat}$ | Photosynthetic photons flux at $ETR_{max}$ | µmol $m^{-2}$ $s^{-1}$ |
| $\Phi_{PSII}$ | Quantum yield of PSII photochemistry | dimensionless |
| $\Phi_{PPFsat}$ | Quantum yield of PSII photochemistry at $PPF_{sat}$ | dimensionless |
| $\alpha'$ | Fraction of light absorbed by PS II | dimensionless |
| $\alpha$ | Initial slope of light response curve of *ETR* | dimensionless |
| $\beta$ | Coefficient of dynamic down-regulation of PSII | dimensionless |
| $\gamma$ | Saturation term of the light response curve for *ETR* | dimensionless |

## Introduction

Needle-leaved evergreen conifers are predominant in Northern Hemisphere forests (Givinish 2002), showcasing their ability to diverse climatic and soil conditions as the primary arboreal and shrub forms across various ecosystems (Neale and Wheeler 2019).

Evergreen conifers have evolved mechanisms to retain needles over multiple years, facilitating sustained photosynthesis even in harsh climates (Givinish 2002; Kivimäenpää and Sutinen 2007; Wyka et al. 2008). Their resilience to extended winter droughts, low temperatures, and poor soil conditions is remarkable. Needle adaptations evolve as they mature (Kivimäenpää and Sutinen 2007; Wyka et al. 2008), with their structural features, including thick epidermis, wax layers, hypodermis, and tracheids, conferring greater drought tolerance compared to broadleaf deciduous trees (Givinish 2002).

Studies have consistently shown a decline in net $CO_2$ assimilation rates with needle age across various conifer species (Freeland 1952; Yoder et al. 1994; Oleksyn et al. 1997; Tissue et al. 2001; Warren 2006; Suzuki and Takahashi 2020). Additionally, factors such as light conditions, temperature, water availability, and nutrient status influence photosynthesis efficiency in conifers. To distinguish the impact of needle age from other factors, we conducted experiments with four evergreen conifer species in common garden conditions.

Changes in needle structure and function with age affect their physiological capabilities (Wang et al. 2022). For instance, older needles of *Pinus sylvestris* L. exhibited lower photosynthetic parameters compared to younger ones (Gielen et al. 2000), attributed to reduced stomatal conductance, nitrogen and chlorophyll concentrations, and glucose accumulation (Coyne and Bingham 1982; Oleksyn et al. 1997; Niinemets 2002; Wu et al. 2021).

While needle age influences photochemical processes during photosynthesis, research on this relationship is limited. Current-year needles in some conifers show lower photochemical efficiency ($F_v/F_m$) compared to one-year-old needles, likely due to transient photoinhibition from excessive light exposure (Jach and Ceulemans 2000). Changes in chlorophyll and carotenoid quantities affect light harvesting and photosynthesis in ageing needles (Adams and Demmig-Adams 1994; Oleksyn et al. 1997), though photoprotective mechanisms, including xanthophyll cycling, remain effective (Adams and Demmig-Adams 1994; Verhoeven 2014). Older needles maintain notable photochemical efficiency, aiding photosynthesis and carbon absorption, especially in low-light environments (Robakowski and Bielinis 2017).

Understanding the long-term needle retention strategy of evergreen conifers is crucial for their adaptation to global climate change, particularly compared to deciduous broadleaf trees. Several studies have explored the effect of needle age on photosynthetic responses to anticipated increases in $CO_2$ concentration (Bazzaz et al. 1993; Wang et al. 1995; Turnbull et al. 1998; Jach and Ceulemans 2000; Wang et al. 2022).

In this study, we investigated needle structure and photochemistry across different age gradients in three evergreen tree species growing under the same habitat conditions. The silver fir (*Abies alba* Mill.), an evergreen conifer prevalent in the hilly areas of central, southern, and eastern Europe (Mauri et al. 2016), was a primary focus. This tree is distinguished by its straight stem and silver-grey trunk (Farjon 2010). Notably, the silver fir maintains the highest number of needle cohorts among European evergreen conifers, with up to 11-12 cohorts. It plays a crucial role in sustaining high biodiversity in forest ecosystems and acts as a functional and ecological stabilizer in European forests. However, the silver fir is particularly susceptible to threats such as fire, insects, fungi, and industrial pollution, especially sulfur dioxide ($SO_2$) exposure during winter (Tinner et al. 2013).

*Taxus baccata* L. is a gymnosperm tree native to western, central, and southern Europe, and it is evergreen and non-resinous. Its population extends sporadically to North Africa and the Middle East (Lewandowski et al. 1995; Rushforth 1999; Thomas and Polwart 2003). The yew tree is the most shade-tolerant among European tree species (Benham et al. 2016). A significant decline in *Taxus baccata* populations motivated us to include this species in our study. The decline has been attributed to various factors, including overexploitation by humans (Piovesan et al. 2009), predation by animals (Farris and Filigheddu 2008; Perrin et al. 2006), excessive shading (Iszkuło and Boratyński 2006; Dhar et al. 2008), and the combined effects of shading and low temperatures.

Norway spruce (*Picea abies* L. Karst.) is a coniferous tree that can grow up to 60 meters tall with a trunk diameter of up to 150 cm. Among the major coniferous species in Europe, Norway spruce has a wide geographic distribution due to its extensive cultivation. It is affected by various natural disturbances, including fires, droughts, storms, and bark beetle infestations. During dry periods, Norway spruce cannot access deep soil water while maintaining transpiration from its 6-8 needle cohorts, which increases its sensitivity to drought (Horgan et al. 2003).

Compared to earlier studies (Robakowski and Bielinis 2017), we focused on needle photochemistry. We extended our research by examining the relationships between needle age,

structure, and photochemistry in three evergreen conifer species growing in a common garden. Our study included trees with more needle age classes (4-8) than previous studies, which typically analyzed only 2-3 needle age classes, with the exception of *Pinus heldreichii* Christ. (8 age classes, Oleksyn et al. 1997), *Pinus densiflora* Sieb. et Zucc. (5 age classes, Han et al. 2008), and *Abies alba* (7 age classes, Robakowski and Bielinis 2017).

We tested the following hypotheses: (1) The leaf-mass-to-area ratio (*LMA*), which reflects leaf structure, would increase as the photosynthetic capacity, expressed as $ETR_{max}$, decreases in ageing and shaded needles. This is consistent with the global relationship between *LMA* and net $CO_2$ assimilation rates, as well as previous studies on other evergreen conifers (Wright et al. 2004). (2) Needle photosynthetic performance would decline with increasing needle age and self-shading within the tree crown. This decline would be indicated by decreases in the maximum quantum yield of PSII photochemistry ($F_v/F_m$), the quantum yield of PSII efficiency ($\Phi_{PSII}$), and the maximal electron transport rate ($ETR_{max}$). Additionally, there would be higher energy losses as heat, reflected by an increase in non-photochemical quenching of fluorescence (*NPQ*) with increasing needle age. (3) Total chlorophyll content would increase, and total carotenoid content would decrease with needle age. This change reflects the functional adaptation of the balance of photosynthetic pigments to the light environment within the tree crown and the senescence processes in needles.

Additionally, due to the self-shading of needles, the $Chl_a/Chl_b$ ratio would decrease with increasing needle age, thereby enhancing the light capture capacity of older and shaded needles (Matsubara et al. 2012; Simkin et al. 2022). These photosynthetic and structural changes in ageing needles would be consistent across different species, reflecting the life strategy of evergreen conifers to maintain their ageing needles and mitigate various stressors.

## Material and Methods

### Study site

The experiment was conducted in the Dendrological Garden (latitude 52° 25’ 37” North, longitude 16° 53’ 48” West, altitude from 70 to 80 m a.s.l), Poznan University of Life Sciences. The soil was sandy, with slightly loamy sand and mid-loamy sand being the predominant soil types in the Garden. The humus layer, which had a pH of 4.5, was made up of decomposing grass roots and leaves of broadleaf and conifer trees. The soil was classed as anthropogenic

rusty soil. The climatic conditions at the site were characterized by mean rainfall of 536 mm, minimum temperature of –28.0°C, and maximum temperature of +38.2°C (Danielewicz 2010).

## Material

Twelve trees (four trees of *A. alba*, *T. baccata* and *P. abies* each) were chosen at the Dendrological Garden of Poznan University of Life Sciences. The study trees were growing with 80% canopy openness under a low shade of other trees. The study trees for each species were growing near each other and had the same size, age, and number of needle age classes. The chosen trees for each species have a long crown (4/5 of a tree's height). *A. alba* and *P. abies* had eight while *T. baccata* had four needle age classes. The lower part of the crowns consisted of needles from every age class. For the needle samples, three shoots were chosen from neighbouring whorls in the lowest section of the tree's south-facing crown. The shoots with the maximum number of needle age classes in the lower part of the crown were selected for sampling of needles. To collect the needle samples for chemical analyses and chlorophyll *a* fluorescence measurements, the centre of each annual shoot increment from the 1- to 8-year-old shoot increment was chosen.

### Measurements of light in tree crown

The measurements of photosynthetic photon flux (*PPF*) were carried out in July (during summer) and in November (during autumn) using two quantum meters (Spectrum Technologies, Inc., Plainfield, USA). The relative photosynthetic photon flux was measured concurrently over a central section of each shoot increment and at an adjacent peripheral area. The following formula was used to derive the relative values: (*PPF* above shoot increment/*PPF* in the open) x 100 and the mean r*PPF* values (r*PPF* – relative photosynthetic photon flux) were derived from three measurements per tree and needle age class and presented in per cent for each needle age class.

### Needle structure

A minimum of 10 needles were selected at a central section of each annual increment representing each age class from the three shoots per tree within 25 days (July – August). While the temperature in the laboratory was around $23^0$C, the mean temperature during the needle sample collection was approximately $22^0$C. Needles were plucked carefully off a twig and inserted into Eppendorf's tubes with a piece of moist filter paper. Next, using a calibrated scanner (Epson Perfection Corp., Seiko, Indonesia), the projected area of the needles was measured with WinSeedle (Regent Inc., Canada). After that, the needles were weighed (fresh weight) and dried at $65^0$C for a week. Leaf mass-to-area ratio (*LMA*) was derived by dividing

needle dry mass per needle area. Three needles from each increment were used to measure chlorophyll *a* fluorescence. Additionally, 40–50 mg fresh mass (*FM* needles) were enclosed into Eppendorf's tubes and placed in a flask containing ice for the spectrophotometric analyses of chlorophyll *a* and *b* and total carotenoid concentration. The samples for pigment analyses were transported using a volume with ice to the Plant Physiology Laboratory on the same day chlorophyll *a* fluorescence was carried out.

### Measurements of chlorophyll *a* fluorescence

The chlorophyll *a* fluorescence in needles was measured using an online Fluorescence Monitoring System (FMS 2, Hansatech, Norfolk, U.K.). Before measurements, the needles were allowed to cool to ambient temperature and adapt to darkness for 30 minutes. The needles were placed within a clip and secured with transparent, self-adhesive tape. Needles were placed on the tape, filling the whole clip's aperture. The needles were subjected to 0.05 μmol $m^{-2}s^{-1}$ modulated measuring light after the fibre optics were inserted into the leaf clip and sealed in a container that could not let light in. To achieve maximum fluorescence ($F_m$), a saturating 0.7s pulse of light ($PPF$ = 15.3 mmol $m^{-2}s^{-1}$) was used after the minimal fluorescence ($F_0$) had been measured. Using the formula maximum quantum yield = $F_v$ /$F_m$, where $F_v$ is the variable fluorescence ($F_v = F_m - F_0$), the maximum quantum yield of PS II photochemistry was calculated.

The needles in the clip were lit with actinic light from an integrated halogen lamp to create light response curves of PSII quantum yield ($\Phi_{PSII}$). After each exposure, a 0.7-second saturation light pulse was applied and the maximum light-adapted fluorescence ($F'_m$) was recorded; this process was repeated up to ten levels of actinic light from 0 to 1415 μmol $m^{-2}$ $s^{-1}$. The goal was to achieve a stable steady-state fluorescence ($F_s$) at each actinic light level before the saturation pulse was applied. The quantum yield of PSII was approximated as $\Phi_{PSII} = (F'_m - F_s)/F'_m$ (Genty et al. 1989). At each actinic light availability, *NPQ* was computed according to the formula: $NPQ = (F_m - F'_m)/F'_m$ (Maxwell and Johnson 2000). Non-photochemical quenching of fluorescence increases infinitely with actinic light. Therefore to compare the values of *NPQ* among the needle age classes and species, we used the *NPQ* values at the level of actinic light of 345 μmol $m^{-2}$ $s^{-1}$.

The apparent rates of photosynthetic electron transport (*ETR*) were calculated using the formula $ETR = \alpha' \times 0.5\ \Phi_{PSII} \times PPF$ for each irradiance with actinic light (Maxwell and Johnson 2000; Lüttge et al. 2003). The excitation energy is split equally between the two photosystems (hence the factor 0.5) (Maxwell and Johnson 2000). However, as needle age grows and self-

shadowing occurs at the tree crown, leaf absorptance ($\alpha'$) may differ along the needle age gradient. Therefore, in our study, leaf absorptance for each needle age class was analysed using the empirical model (Evans 1993), which is based on the total chlorophyll content of the leaf. Light curves of fluorescence were generated for each study species, tree, shoot and needle age class. In total, 240 light curves of fluorescence were generated; for *A. alba* and *P. abies* two species x 4 trees x 3 shoots x 8 needle age classes = 192; for *T. baccata* four trees x 3 shoots x 4 needle age classes = 48 light curves.

## Modelling of light curves

To determine the relationship between *ETR* and *PPF*, the equation was fitted to the data through the nonlinear regression (Ye et al. 2013):

$$ETR = \alpha \frac{1 - \beta \times PPF}{1 + \gamma \times PPF} PPF,$$

where $\alpha$ is the initial slope, $\gamma$ is the saturation term of the light response curve for the photosynthetic electron transport rate (*ETR- PPF*), and $\beta$ is the degree of dynamic down-regulation of PSII, *PPF* is photosynthetic photon flux of actinic light.

To determine the cardinal points of the light curves of the $\Phi_{PSII}$ and *ETR*, Ye et al. (2013) models were utilised to compare light responses among the species and the needle age classes. The quantum yield of PSII photochemistry at saturating *PPF* ($\Phi_{PPFsat}$) (1), the saturating value of photosynthetic photon flux at which $ETR = ETR_{max}$ ($PPF_{sat}$) (2), and the maximum apparent rate of photosynthetic electron transport of PSII ($ETR_{max}$) (3) were also estimated using the Ye et al. (2013) models.

$$\Phi_{\mathrm{PPFsat}} = \frac{\alpha}{0.5 \times \alpha'} \times \frac{1 - \beta \times PPF_{\mathrm{sat}}}{1 + \gamma \times PPF_{\mathrm{sat}}} \quad (1)$$

Here, the value of 0.5 comes from the assumption that the excitation energy is equally divided between the two photosystems, $\alpha'$ represents the value of leaf absorptance.

$$PPF_{\mathrm{sat}} = \frac{\sqrt{(\beta+\gamma)/\beta} - 1}{\gamma} \quad (2)$$

$$ETR_{\mathrm{max}} = \alpha \left( \frac{\sqrt{\beta + \gamma} - \sqrt{\beta}}{\gamma} \right)^2 \quad (3)$$

The model was fitted to the empirical data and the values of cardinal points of light curves were calculated using the Photosynthesis Model Simulation Software at http://photosynthetic.sinaapp.com/index.html.

## Spectral analysis of photosynthetic pigments

Spectrophotometric analyses were performed on 240 needle samples to determine the levels of total carotenoids, total chlorophyll, chlorophyll *a*, and chlorophyll *b*. These assessments were carried out concurrently with measurements of chlorophyll *a* fluorescence on the same days. Photosynthetic pigments were estimated using the Hiscox and Israelstam method (1979). Needles (40 – 50 mg fresh mass (FM) from each needle age class (increment) along a branch were collected and taken to the laboratory. Needles were cut into 2 mm pieces, treated with 5 mL dimethylsulfoxide (DMSO) and incubated for 60 min in a water bath at 65 °C. The absorbance of extracts was measured at 663, 645, and 480 nm. If absorbance values were higher than 0.7, the extract was diluted accordingly. The pigment content was calculated using modified Arnon formulas (Welburn 1994) and expressed in milligrams per gram of fresh weight. Physiological parameters were measured spectrophotometrically (Jasco V-530 UV-VIS). The pigments were recalculated per needle dry mass and needle area using fresh to dry mass ratio and *LMA*.

## Statistical analyses

The linear or polynomial regression was applied to show the relationships between the needle age classes, the values of r*PPF*, photochemical parameters and photosynthetic pigment contents. The regression models were fitted to the mean values for each species and needle age class in SigmaPlot v. 13.0 (Sysstat Software, Inc.). Prior to the analyses of variance, the mean values of each parameter per tree and needle age class were calculated ($n = 4$, $n$ – number of trees per species). Data were tested for normality and homogeneity using Shapiro-Wilk and Levene's tests. Data which did not fulfill the ANOVA conditions were log-transformed. The mixed model of analysis of variance with the "species" and "needle age class" as the fixed factors and the "tree" as the random factor was conducted at $P < 0.05$ in *R* (R Core Team 2024). The applied mixed model of ANOVA was as follows: $Y_{ijk} = \mu + \alpha_i + \beta_j + \gamma_k + \epsilon_{ijk}$ , where: $Y_{ijk}$ – the response variable for the *i*th level of the first fixed factor, the *j*th level of the second fixed factor, and the *k*th observation within the (*i*, *j*) combination; $\mu$ – the overall mean; $\alpha_i$ – the effect of the *i*th level of the first fixed factor; $\beta_j$ – the effect of the *j*th level of the second fixed factor; $\gamma_k$ – the random effect associated with the *k*th observation; $\epsilon_{ijk}$ – the random error term associated with the (*i*, *j*, *k*) observation, assumed to be independent and normally distributed with mean 0 and constant variance $\sigma^2$. The package *lme4* was used for the mixed ANOVA (Bates et al. 2015), and the packages *lmerTest* and *emmeans* for post-hoc comparisons with Tukey's method at $\alpha = 0.05$ (Kuznetsova et al., 2017; Lenth 2024).

The needle age class and tree were used as independent variables in a two-way analysis of variance (ANOVA) with the interaction. The interaction between the needle age class (fixed factor) and tree (random factor) was used as an error term in one-way ANOVA with the needle age class as the categorical variable ($P < 0.05$). Then, the means were separated by Tukey's test at $\alpha < 0.05$.

## Results

### Light levels above shoots and needle structure

The relative values of photosynthetic photon flux (r*PPF*) decreased linearly from the youngest shoot increment horizontally within the crowns of *A. alba*, *T. baccata*, and *P. abies* (Fig. 1a). However, the decrease in light levels was more rapid for *A. alba* and *T. baccata*, showing lower negative slope values in linear regression compared to *P. abies*. The light level above the annual shoot increments decreased from the crown periphery (youngest needles) to the trunk (oldest needles), regardless of species. However, r*PPF* values depended on the overall light environment and the species-specific and individual tree crown structure. *Aabies alba* exhibited higher *LMA* compared to both *P. abies* and *T. baccata*, with no significant differences observed between the latter two. The correlation between mean *LMA* values and needle age shows an exponential increase to the maximum in *A. alba* and *P. abies*, but this pattern was not significant for *T. baccata* (Fig. 1b).

### Impact of needle age on photochemistry

The maximum quantum yield of PSII photochemistry ($F_v/F_m$) decreased linearly with needle age (Table 1, Fig. 2a). This trend was significant for *Taxus* and *Picea*, but not for *Abies*, indicating significant interspecific differences in the $F_v/F_m$ decrease with needle age (Table S1). Despite this decline, the mean values of $F_v/F_m$ remained above 0.80 across all species and needle ages, indicating a lack of photoinhibition even in the oldest needles. Similarly, for $ETR_{max}$, a significant decreasing linear relationship was observed with needle age across the species. *A. alba* consistently exhibited higher $ETR_{max}$ values than both *Taxus* and *Picea* at each needle age class (Tables 1, S1, Fig. 2b).

It was observed that the values of *NPQ* increased linearly with needle age, except for *T. baccata*, which did not show a significant trend, likely due to the lower number of needle cohorts compared to the other study species (Fig. 2c). *A. alba* and *P. abies* exhibited higher *NPQ* values than *T. baccata* (Table S1, Fig. 2c).

There wasn't a significant relationship between the mean values of the quantum yield of PSII photochemistry at the saturation level of actinic light ($\Phi_{PFFsat}$) and increasing needle age within the study species (Table 1, Fig. 3a). However, *A. alba* consistently exhibited the highest $\Phi_{PFFsat}$ among the species regardless of needle age class, except for the oldest needles (Table S1, Fig. 3a). In contrast, there were significant linear (*P. abies*) or parabolic (*A. alba*, *T. baccata*) decreasing trends for the saturation level of *PPF* ($PPF_{sat}$) without differences among the species and needle age classes (Tables 1 and S1, Fig. 3b). This indicates that aging needles progressively adapted to increasing self-shading from the crown periphery to the trunk.

### Photosyntetic pigment content in ageing needles

Significant differences were observed in the amount of photosynthetic pigments in needles among the study species (Table S2). Total chlorophyll concentration (mg $g^{-1}$) was not significantly related to needle age classes for *A. alba* and *P. abies*. However, a downward parabolic relationship was evident for *T. baccata* (Fig. 4a). Regarding total carotenoid concentration (mg $g^{-1}$), no significant differences were observed in the species' relationship with needle age. However, *T. baccata* and *P. abies* exhibited higher values than *A. alba* in each needle age class (Table S2, Fig. 5a). We observed a significant relationship in total carotenoids content (g $m^{-2}$) for *A. alba*, while no significant relationship was found for *T. baccata* and *P. abies*. A decreasing trend with age was observed in *T. baccata*, while a non-significant trend was observed in *A. alba* and *P. abies* for the ratio of total carotenoids content to total chlorophyll content (Fig. 5c). Concerning chlorophyll content, we noted noticeable changes as needle age increased. As the needles aged, the overall chlorophyll content (i.e., chlorophyll *a* and *b*) tended to increase and then subsequently decrease, while the ratio of $Chl_a/Chl_b$ decreased linearly with increasing age regardless of the species (Table S2, Fig. 6).

## Discussion

### *Influence of needle age and light levels on needle structure*

The evergreen coniferous tree species in our study - *A. alba*, *P. abies*, and *T. baccata* - represent the slow-return end of the leaf economics spectrum. These species have long leaf lifetimes, costly high-*LMA* leaf construction, low nutrient concentrations, and low rates of photosynthesis and respiration (Wright et al. 2004). Our study provides evidence that their needle structure and photosynthetic patterns change with needle age, following the decreasing horizontal light trend within the crown.

When we compared the variability of *LMA* among different needle cohorts, it partly aligned with the concept of needle acclimation to varying light conditions (Ishii et al. 2006). However, in our study, the relationship between *LMA* and the combined impact of age and light level was non-linear. We observed a rapid increase in this ratio in young needles, stabilization at the needle maturation stage, and in the case of *T. baccata* and *P. abies*, even a remarkable decrease of *LMA* in the oldest needles. These findings suggest that needles transition from fast resource acquisition to resource conservation during development, illustrating the 'fast-slow' plant economics spectrum within individual evergreen trees (Reich 2014). During expansion, young needles generally have a lower construction cost with increasing needle area due to volumetric increases in cell size rather than the addition of significant amounts of cell wall materials. Conversely, during leaf maturation, the apoplastic volume fraction increases relative to the symplastic volume fraction due to the deposition of secondary cell wall materials, including the lignification of vascular tissues. This phenomenon, observed across leaf age groups of *Photinia* X *fraseri* "Red Robin," aligns with the *LMA* trends in our study species (Jiao et al. 2022).

The structural changes that occur in needles with age are directly reflected in *LMA*. Generally, *LMA* tends to increase with needle age up to the fourth needle age class, indicating that older needles may possess a denser or thicker composition than younger ones, as demonstrated in previous studies (Niinemets et al. 2004; Huo and Wang 2007; Han et al. 2008; Wu et al. 2022). Although the observed changes in *LMA* were consistent across all our study species, their dynamics depended on the species-related crown structure and in-crown light conditions (Table S1).

*Photochemistry*

In our study, the values of $F_v/F_m$ varied within a narrow range depending on the species and needle age class. This suggests that the high plasticity of needles in response to their increasing age and self-shading is reflected in their ability to maintain $F_v/F_m$ above the photoinhibitory threshold across needle age classes. The maximum quantum yield of PSII photochemistry showed a decreasing linear trend in *P. abies* and *T. baccata* with needle age and differed among needle age classes within the species, except for *A. alba*. This indicates that the combined effect of needle age and light on $F_v/F_m$ is species-specific (Table S1, Fig. 2a). Similar changes in $F_v/F_m$ have also been observed in *Pinus pumila* (Amagai et al. 2015), further supporting our findings.

The values of $ETR_{max}$ in *A. alba*, *T. baccata*, and *P. abies* declined linearly with increasing needle age, and $\Phi_{PPFsat}$ did not significantly vary among the needle cohorts (Fig. 3). The decrease observed in $ETR_{max}$ with needle age was not due to photoinhibition but was associated with a significant decrease in $PPF_{sat}$, slight PSII downregulation, and increasing *NPQ*. Our results showed that even old needles sustained the ability of PSII to convert light energy. This is consistent with previous reports for evergreen species such as *Pinus heldrechii*, *Pinus sylvestris*, *Pinus pinaster* Aiton, *Ilex aquifolium* L., and *Quercus ilex* L. (Oleksyn et al. 1997; Niinemets and Valladares 2006; Warren 2006). Earlier studies indicated that as needles aged, there was a predictable and continuous decrease in net $CO_2$ assimilation rates, stomatal conductance, transpiration rates, and glucose accumulation (Oleksyn et al. 1997; Robakowski and Bielinis 2017). Our results provide evidence that the decreasing carbon sink in ageing needles might give negative feedback, reducing *ETR* and enhancing *NPQ* in ageing needles.

The saturation photosynthetic photon flux level ($PPF_{sat}$) decreased with needle age, indicating an adaptation to the self-shading of branches in the tree crown (Fig. 3). This suggests that as needles aged, they required lower values of *PPF* to achieve $ETR_{max}$. This finding aligns with Wyka et al. (2008), who reported that older *T. baccata* needles were less susceptible to photoinhibition and had lower *ETR* than needles from the current year. This phenomenon underscores the ability of evergreen conifers to adapt to varying light levels and optimize photosynthetic capacity by retaining numerous cohorts of needles in response to external conditions.

*Needle pigments*

In our study, differences in pigment concentration among species and needle age classes depended on needle structure, which was reflected in leaf mass per area (*LMA*). When total chlorophyll was recalculated per needle dry mass, it revealed an upward parabolic-like trend as the needles aged, whereas recalculating per needle area showed a downward parabolic trend (Fig. 4). The variations in total chlorophyll levels across the three study species could indicate distinct responses modified by species-specific crown structure and needle age. The observed decrease and subsequent increase in $Chl_{tot}$ per unit dry mass for all tree species align with physiological and anatomical changes in needles driven by varying light levels associated with increasing needle age (Fig. 4) (Han et al. 2008; Kuusk et al. 2018).

We observed a downward parabolic trend in $Chl_a$ and $Chl_b$ content versus needle age for *A. alba*, *T. baccata*, and *P. abies*, along with a negative linear trend in the ratio of $Chl_a/Chl_b$ (Fig. 6). However, the coefficient "b" in the parabolic equations for $Chl_a$ was three times higher than for $Chl_b$, indicating that $Chl_b$ varied less with needle age compared to $Chl_a$.

Our results are consistent with Evans (1995), who found that a declining $Chl_a/Chl_b$ ratio resulted from greater investment in the Light-Harvesting Complex (LHC), possibly associated with alterations in the plant's photosynthetic mechanism, particularly in terms of light absorption and energy transfer efficiency (Simkin et al. 2022). As needles age, they become increasingly shaded by shoots in the crown and adapt to capture more dispersed light. Chlorophyll *a* and *b* differ in their wavelength of light absorption maxima, hence the decreasing ratio of $Chl_a/Chl_b$ increases the ability of senescent needles to capture more blue and yellow light, whereas $Chl_a$ absorbs more violet and orange light (Simkin et al. 2022). The $Chl_a/Chl_b$ ratio informs about the plant's efficiency in utilizing different wavelengths of light and in electron transfer efficiency (Kang et al. 2022). Chlorophyll *b* tends to absorb scattered solar radiation complementary to $Chl_a$, thereby increasing the absorption capacity of old and shaded needles exposed to more diffuse solar radiation in the tree crown compared to younger needles exposed to light with a greater proportion of direct radiation. The ratio of $Chl_a/Chl_b$ influences the light-capturing effectiveness of a plant. It appears that the balance between photosynthetic pigments, specifically $Chl_a/Chl_b$ and $Car/Chl_{tot}$ ratios during needle ageing and structural development, was influenced by varying proportions of direct and diffuse sunlight illuminating needles, a factor considered a driver of plant evolution (Kume et al., 2018).

Total carotenoid levels in *A. alba*, *T. baccata*, and *P. abies* increased during the early phases of needle growth and then decreased with age following changes in $Chl_{tot}$ (Fig. 5). This decline may be linked to increasing self-shading within the crown and age-related changes in the physiological processes of the needles. In our study, *T. baccata* had the smallest number of needle age classes, and individuals of this species grew predominantly in low shade, which might result in a lower number of needle cohorts. Generally, young needles had higher total carotenoid concentrations compared with older needles, which can be explained by their photoprotective role in needles exposed to higher light levels than older needles (Adams et al. 2004; Demmig-Adams and Adams 2006). The ratio of $Car/Chl_{tot}$ remained stable in *A. alba* or decreased with needle age in *T. baccata* and *P. abies*, confirming the adaptation of needles to the light environment in the crown.

*Evolutionary significance of needle adaptations in response to global climate change*

Evergreen conifers, including our study species *A. alba*, *T. baccata*, and *P. Abies*, have developed various survival mechanisms to endure adverse climatic conditions such as drought, cold temperatures, and nutrient scarcity, ensuring continuous photosynthesis throughout the

year (Wyka and Oleksyn 2014; Liu et al. 2024; Verhoeven and Kornkven 2024). Our research reveals that ageing needles maintain high PSII efficiency, dynamically adjust the $Chl_a/Chl_b$ ratio and $Car/Chl_{tot}$ ratio to effectively capture light in changing light environments, and manage their energetic budget to compromise photosynthetic capacity with varying light conditions and energy partitioning among different photosynthetic processes and losses.

Oleksyn et al. (2020) demonstrated that across a 1000 km transect in Scots pine forests in Sweden, plants in modern conditions (*circa* 2015), growing in 1°C warmer climates, have longer needles and shorter needle lifespans compared to plants a century ago (*circa* 1915). This century-scale change in needle lifespan suggests that adaptation of evergreen conifers to climate warming may involve shortening needle lifespan. Evergreen plants in high latitudes, where low temperatures limit photosynthesis, can maintain high rates of *NPQ* (Verhoeven 2014). Under normal conditions, *NPQ* raises leaf temperature by less than 0.1°C, but it can increase to 1°C under specific conditions (Murakami et al. 2024). However, the potential positive effects of temperature increase due to *NPQ* on photosynthesis or other physiological processes in evergreen conifers have not been demonstrated. This knowledge gap underscores potential future research directions. Our findings indicate that heat loss as *NPQ* increases with needle age in *A. alba* and *P. abies*. Thus, in evergreen conifers, shading and low temperatures induce a potential energy imbalance by downregulating biochemical reactions of the Calvin-Benson cycle in old needles, which cannot be compensated by an increase in temperature due to heat dissipation. Retention of old needles with high *NPQ* may become photosynthetically inefficient under rising air temperatures. A smaller number of cohorts of young, long needles with higher $ETR_{max}$ and lower *NPQ* values may be better adapted to climate warming, aligning with Oleksyn et al. (2020).

Our findings, along with those of Oleksyn et al. (2020), suggest that under conditions where air temperature is less limiting for photosynthesis due to climate warming, evergreen coniferous trees might sustain or even increase photosynthetic intensity by shortening needle lifespan. Our results suggest that this adjustment would reduce energy losses as heat and enhance the overall energy balance in tree photosynthesis. We also observe interspecific differences in needle retention ability. Additionally, the age and light-related gradients of structural and functional patterns of needles vary among species, highlighting the importance of considering these factors when predicting the responses of evergreen conifers to global climate changes.

## Supplementary Information

Table S1. The results of the mixed analysis of variance with the photochemical parameters as dependent variables, the species and needle age class (cohort) as the fixed factors and the tree as the random factor ($P < 0.05$).

Table S2. The results of the mixed analysis of variance with *LMA* – leaf mass-to-area ratio (g $m^{-2}$), total chlorophyll concentration (mg $g^{-1}$), total chlorophyll content (g $m^{-2}$), chlorophyll *a*, *b* (mg $g^{-1}$; g $m^{-2}$), chlorophyll *a*/*b* ratio, total carotenoids (mg $g^{-1}$; g $m^{-2}$) and total carotenoids / chlorophyll ratio as dependent variables, the species and needle age class (cohort) as the fixed factors and the tree as the random factor ($P < 0.05$).

## Funding

This research was supported by Faculty of Forestry and Wood Technology, Poznań University of Life Sciences, Poznań, Poland.

## Author Contributions

Material preparation, morphological and fluorescence measurements, and data analyses were performed by James Oluborode. Pigment analyses were conducted by Tamara Chadzinikolau and Magda Formela-Luboińska. Zi-Piao Ye provided the software for modeling of light curves and verified the analyses. The first draft of the manuscript was written by James Oluborode. All authors commented on previous versions of the manuscript and approved the final version. Piotr Robakowski conceived the study and supervised the project.

## Declaration

The authors have no relevant financial or non-financial interests to disclose.

## Bibliography

Adams WW, Demmig-Adams B (1994) Carotenoid composition and down regulation of photosystem II in three conifer species during the winter. Physiol Plant 92(3):451–458. https://doi.org/10.1111/j.1399-3054.1994.tb08835.x

Adams WW, Zarter CR, Ebbert V, Demmig-Adams B (2004) Photoprotective strategies of overwintering evergreens. Bioscence, 54(1):41–49. https://doi.org/10.1641/0006-3568(2004)054[0041:PSOOE]2.0.CO;2

Amagai Y, Kaneko M, Kudo G (2015) Habitat-specific responses of shoot growth and distribution of alpine dwarf-pine (*Pinus pumila*) to climate variation. Ecol Res 30:969–977. https://api.semanticscholar.org/CorpusID:7521769

Bates D, Mächler M, Bolker B, Walker S (2015) Fitting Linear Mixed-Effects Models Using lme4. J Stat Softw 67(1). https://doi.org/10.18637/jss.v067.i01

539 Bazzaz FA, Miao S, Wayne PM (1993) $CO_2$-induced growth enhancements of co-occurring tree species
540 decline at different rates. Oecologia 96(4):478–482. https://api.semanticscholar.org/CorpusID:8688992

541 Benham SE, Houston Durrant T, Caudullo G, de Rigo D (2016) *Taxus baccata* in Europe: Distribution,
542 habitat, usage and threats. In: San-Miguel-Ayanz J, de Rigo D, Caudullo G, Houston Durrant T, Mauri
543 A (eds) European Atlas of Forest Tree Species. Publication Ofce of the EU, Luxembourg, p e015921

544 Coyne PI, Bingham GE (1982) Variation in Photosynthesis and Stomatal Conductance in an Ozone-
545 Stressed Ponderosa Pine Stand: Light Response. For Sci 28(2):257–273.
546 https://doi.org/10.1093/FORESTSCIENCE/28.2.257

547 Danielewicz W (2010) *Folder_Ogr_Dendr*. http://panbook.pl/wp-
548 content/uploads/2015/02/Folder_Ogr_Dendr.pdf

549 Demmig-Adams B, Adams III WW (2006) Photoprotection in an ecological context: the remarkable
550 complexity of thermal energy dissipation. New Phytol 172(1):11–21. https://doi.org/10.1111/j.1469-
551 8137.2006.01835.x

552 Dhar A, Ruprecht H, Vacik H (2008) Population viability risk management (PVRM) for in situ management
553 of endangered tree species—A case study on a *Taxus baccata* L. population. For Ecol and Manag
554 255(7): 2835–2845. https://doi.org/https://doi.org/10.1016/j.foreco.2008.01.059

555 Evans J (1993) Photosynthetic Acclimation and Nitrogen Partitioning Within a Lucerne Canopy. I. Canopy
556 Characteristics. Funct Plant Biol 20(1):55–67. https://doi.org/10.1071/PP9930055

557 Evans J (1995) Carbon Fixation Profiles Do Reflect Light Absorption Profiles in Leaves. Funct Plant Biol
558 22:865–873. https://doi.org/10.1071/PP9950865

559 Farjon A (2010) A Handbook of the World's Conifers. Brill, Leiden, The Netherlands.
560 https://doi.org/10.1163/9789047430629

561 Farris E, Filigheddu R (2008) Effects of browsing in relation to vegetation cover on common yew (*Taxus*
562 *baccata* L.) recruitment in Mediterranean environments. Plant Ecol 199(2):309–318.
563 https://doi.org/10.1007/s11258-008-9434-x

564 Freeland RO (1952) Effect of age of leaves upon the rate of photosynthesis in some conifers. Plant Physiol
565 27(4):685–690.

566 Genty B, Briantais JM, Baker NR (1989) The relationship between the quantum yield of photosynthetic
567 electron transport and quenching of chlorophyll fluorescence. Biochim et Biophys Acta (BBA) - Gen
568 Subj 990(1):87–92. https://doi.org/10.1016/S0304-4165(89)80016-9

569 Gielen B, Jach M, Ceulemans R (2000) Effects of season, needle age, and elevated atmospheric $CO_2$ on
570 chlorophyll fluorescence parameters and needle nitrogen concentration in Scots pine (*Pinus sylvestris*).
571 Photosynthetica 38:13–21

572 Givinish T (2002) Adaptive significance of evergreen vs. deciduous leaves: solving the triple paradox. Silva
573 Fenn 36(3):703–743. https://doi.org/10.14214/sf.535

574 Grassi G, Colom MR, Minotta G (2001) Effects of nutrient supply on photosynthetic acclimation and
575 photoinhibition of one-year-old foliage of *Picea abies*. Physiol Plant 111(2):245–254.
576 https://doi.org/10.1034/j.1399-3054.2001.1110217.x

577 Han Q, Kawasaki T, Nakano T, Chiba Y (2008) Leaf-age effects on seasonal variability in photosynthetic
578 parameters and its relationships with leaf mass per area and leaf nitrogen concentration within a *Pinus*
579 *densiflora* crown. Tree Physiol 28(4):551–558. https://doi.org/10.1093/treephys/28.4.551

Hiscox JD, Israelstam GF (1979) A method for the extraction of chlorophyll from leaf tissue without maceration. Can J Bot 57(12):1332–1334. https://doi.org/10.1139/b79-163

Horgan T, Keane M, McCarthy R, Lally M, Thompson D, O'Carroll J (2003) A guide to forest tree species selection and silviculture in Ireland. National Council for Forest Research and Development (COFORD)

Huo H, Wang C (2007) Effects of canopy position and leaf age on photosynthesis and transpiration of *Pinus koraiensis*. J Appl Ecol 18:1181–1186.

Ishii Y, Sakamoto K, Yamanaka N, Wang L, Yoshikawa K (2006) Light acclimation of needle pigment composition in *Sabina vulgaris* seedlings under nurse plant canopy. J Arid Environ 67(3):403–415. https://doi.org/10.1016/j.jaridenv.2006.03.004

Iszkuło G, Boratyński A (2006) Analysis of the relationship between photosynthetic photon flux density and natural *Taxus baccata* seedlings occurrence. Acta Oecol 29(1):78–84. https://doi.org/10.1016/j.actao.2005.08.001

Jach M, Ceulemans R (2000) Effects of season, needle age and elevated atmospheric $CO_2$ on photosynthesis in Scots pine (*Pinus sylvestris*). Tree Physiol 20(3):145–157. https://doi.org/10.1093/treephys/20.3.145

Jiao Y, Niklas KJ, Wang L, Yu K, Li Y, Shi P (2022) Influence of Leaf Age on the Scaling Relationships of Lamina Mass vs. Area. Front Plant Sci 13:860206. https://doi.org/10.3389/fpls.2022.860206

Kalaji HM, Schansker G, Brestic M, et al (2017) Frequently asked questions about chlorophyll fluorescence, the sequel. Photosynth Res 132:13-66. https://doi.org/10.1007/s11120-016-0318-y

Kang JH, Yoon HI, Lee JM, et al (2022) Electron transport and photosynthetic performance in Fragaria x ananassa Duch. Acclimated to the solar spectrum modified by a spectrum conversion film. Photosynth Res 15(1):31–46. https://doi.org/10.1007/s11120-021-00875-7

Kivimäenpää M, Sutinen S (2007) Microscopic structure of Scots pine (*Pinus sylvestris* (L.)) needles during ageing and autumnal senescence. Trees - Structure and Function, 21(6):645–659. https://doi.org/10.1007/s00468-007-0157-8

Kume A, Akitsu T, Nasahara KN (2018) Why is chlorophyll b only used in light-harvesting systems? J Plant Res 131:961–972. https://doi.org/10.1007/s10265-018-1052-s

Kuusk V, Niinemets Ü, Valladares F (2018) A major trade-off between structural and photosynthetic investments operative across plant and needle ages in three Mediterranean pines. Tree Physiol 38(4):543–547. https://doi.org/10.1093/treephys/tpx139

Kuznetsova A, Brockhoff PB, Christensen RHB (2017) lmerTest Package: Tests in Linear Mixed Effects Models. J Stat Softw 82(13). https://doi.org/10.18637/jss.v082.i13

Liu M, Wang Y, Zhang H, Hao Y, Wua H, Shen H, Zhang P (2024) Mechanisms of photoprotection in overwintering evergreen conifers: Sustained quenching of chlorophyll fluorescence. Plant Physiol Biochem 108638. https://doi.org/10.1016/j.plaphy.2024.108638

Lenth R (2024) *emmeans: Estimated Marginal Means, aka Least-Squares Means_. R package version 1.10.1, <https://CRAN.R-project.org/package=emmeans>*.

Lewandowski A, Burczyk J, Mejnartowicz LE (1995) Genetic structure of English yew (*Taxus baccata* L.) in the Wierzchlas Reserve: implications for genetic conservation. For Ecol Manag 73(1-3):221–227. https://api.semanticscholar.org/CorpusID:84469518

Lüttge U, Berg A, Fetene M, Nauke P, Peter D, Beck E (2003) Comparative characterization of photosynthetic performance and water relations of native trees and exotic plantation trees in an Ethiopian forest. Trees, 17(1):40–50. https://doi.org/10.1007/s00468-002-0201-7

Matsubara S, Förster B, Waterman M, et al (2012) From ecophysiology to phenomics: some implications of photoprotection and shade–sun acclimation in situ for dynamics of thylakoids in vitro. Philos Trans R Soc Lond B Biol Sci 367(1608):3503-3514. https://doi.org/10.1098/RSTB.2012.0072

Mauri A, de Rigo D, Caudullo G (2016) *Abies alba* in Europe: distribution, habitat, usage and threats. European Atlas of Forest Tree Species 48-49.

Maxwell K, Johnson GN (2000) Chlorophyll fluorescence—a practical guide. J Exp Bot 51(345), 659–668. https://doi.org/10.1093/jexbot/51.345.659

Neale DB, Wheeler NC (2019) The conifers: (pp. 1-21). Springer International Publishing. https://doi.org/10.1007/978-3-319-46807-5_1

Niinemets U (2002) Stomatal conductance alone does not explain the decline in foliar photosynthetic rates with increasing tree age and size in *Picea abies* and *Pinus sylvestris*. Tree Physiol, 22(8):515–535. https://doi.org/10.1093/treephys/22.8.515

Niinemets Ü, Tenhunen J, Beyschlag W (2004) Spatial and age-dependent modifications of photosynthetic capacity in four Mediterranean oak species. Funct Plant Biol 31(12):1179–1193. https://api.semanticscholar.org/CorpusID:85165792

Niinemets Ü, Valladares F (2006) Tolerance to shade, drought, and waterlogging of temperate Northern Hemisphere trees and shrubs. Ecol Monogr 76(4):521–547. https://doi.org/10.1890/0012-9615(2006)076[0521:TTSDAW]2.0.CO;2

Oleksyn J, Tjoelker MG, Lorenc-Plucińska G, Konwińska A, Zytkowiak R, Karolewski P, Reich PB (1997) Needle $CO_2$ exchange, structure and defense traits in relation to needle age in *Pinus heldreichii* Christ - A relict of Tertiary flora. Trees 12(2):82–89. https://doi.org/10.1007/PL00009700/METRICS

Oleksyn J, Wyka TP, Żytkowiak R, Zadworny M, et al (2020) A fingerprint of climate change across pine forests of Sweden. Eol Lett 23(12):1739-1746. https://doi.org/10.1111/ele.13587

Perrin PM, Kelly DL, Mitchell FJG (2006) Long-term deer exclusion in yew-wood and oakwood habitats in southwest Ireland: Natural regeneration and stand dynamics. Forest Ecol and Manag 236(2–3):356–367. https://doi.org/10.1016/j.foreco.2006.09.025

Piovesan G, Presutti SE, Biondi F, Alessandrini A, Di Filippo A, Schirone B (2009) Population ecology of yew (*Taxus baccata* L.) in the Central Apennines: spatial patterns and their relevance for conservation strategies. Plant Ecol 205(1):23–46. https://doi.org/10.1007/s11258-009-9596-1

R Core Team (2024) R: A Language and Environment for Statistical Computing_. R Foundation for Statistical Computing, Vienna, Austria. https://www.R-project.org

Reich PB (2014) The world-wide "fast-slow" plant economics spectrum: A traits manifesto. J Ecol 102(2):275–301. https://doi.org/10.1111/1365-2745.12211

Robakowski P, Bielinis E (2017) Needle age dependence of photosynthesis along a light gradient within an *Abies alba* crown. Acta Physiol Plant 39:1-12. https://doi.org/10.1007/s11738-017-2376-y

Rushforth K D (1999). Collins Wildlife Trust Guide: Trees: A Photographic Guide to the Trees of Britain and Europe. HarperCollins. New York USA. ISBN 0002200139.

Simkin AJ, Kapoor L, Doss CGP, Hofmann TA, Lawson T, Ramamoorthy S (2022) The role of photosynthesis related pigments in light harvesting, photoprotection and enhancement of photosynthetic yield in planta. Photosynth Res 152(1):23–42. https://doi.org/10.1007/s11120-021-00892-6

662 Suzuki R, Takahashi K (2020) Effects of leaf age, elevation and light conditions on photosynthesis and leaf
663 traits in saplings of two evergreen conifers, *Abies veitchii* and *Abies mariesii*. J Plant Ecol 13(4):460–
664 469. https://doi.org/10.1093/jpe/rtaa034

665 Thomas PA, Polwart A (2003) *Taxus baccata* L. J Ecol 91(3):489–524. https://doi.org/10.1046/j.1365-
666 2745.2003.00783.x

667 Tinner W, Colombaroli D, Heiri O, Henne PD, Steinacher M, Untenecker J, Vescovi E, Allen JRM, Carraro
668 G, Conedera M, Joos F, Lotter AF, Luterbacher J, Samartin S, Valsecchi V (2013) The past ecology of
669 *Abies alba* provides new perspectives on future responses of silver fir forests to global warming. Ecol
670 Monogr 83(4):419–439. https://doi.org/10.1890/12-2231.1

671 Tissue DT, Griffin KL, Turnbull MH, Whitehead D (2001) Canopy position and needle age affect
672 photosynthetic response in field-grown *Pinus radiata* after five years of exposure to elevated carbon
673 dioxide partial pressure. Tree Physiol 21(12–13):915–923. https://doi.org/10.1093/TREEPHYS/21.12-
674 13.915

675 Turnbull MH, Tissue DT, Griffin KL, Rogers GND, Whitehead D (1998) Photosynthetic acclimation to
676 long-term exposure to elevated $CO_2$ concentration in *Pinus radiata* D. Don. is related to age of needles.
677 Plant Cell Environ 21:1019–1028. https://api.semanticscholar.org/CorpusID:84893703

678 Verhoeven A (2014) Sustained energy dissipation in winter evergreens. New Phytol 201(1):57–65.
679 https://doi.org/10.1111/nph.12466

680 Verhoeven A, Kornkven J (2024) Differences in photoprotective strategy during winter in Eastern white
681 pine and white spruce. Tree Physiol 44, tpad131. https://doi.org/10.1093/treephys/tpad131

682 Wang J, Ouyang F, An S, Wang L, Xu N, Ma J, Wang J, Zhang H, Kong L (2022) Variation, coordination,
683 and trade-offs between needle structures and photosynthetic-related traits across five *Picea* species:
684 consequences on plant growth. BMC Plant Biol 22(1):1–16. https://doi.org/10.1186/S12870-022-
685 03593-X

686 Wang K, Kellomaki S, Laitinen K (1995) Effects of needle age, long-term temperature and $CO_2$ treatments
687 on the photosynthesis of Scots pine. Tree Physiol 15(4):211–218.
688 https://doi.org/10.1093/treephys/15.4.211

689 Warren CR (2006) Why does photosynthesis decrease with needle age in *Pinus pinaster*? Trees 20(2):157–
690 164. https://doi.org/10.1007/s00468-005-0021-7

691 Wellburn AR (1994) The spectral determination of chlorophylls a and b, as well as total carotenoids, using
692 various solvents withspectrophotometers of different resolution. J Plant Physiol 144(3):307–313.
693 https://doi.org/10.1016/S0176-1617(11)81192-2

694 Wright IJ, Reich PB, Westoby M, Ackerly DD, Baruch Z, Bongers F, Cavender-Bares J, Chapin T,
695 Cornelissen JHC, Diemer M, Flexas J, Garnier E, Groom PK, Gulias J, Hikosaka K, Lamont BB, Lee
696 T, Lee W, Lusk C, Villar R (2004) The worldwide leaf economics spectrum. Nature 428(6985):821–
697 827. https://doi.org/10.1038/nature02403

698 Wu H, Yin D, Rodríguez-Calcerrada J, Zhang J, Gil L, Zhang P, Shen H (2022) Cone-bearing effects on
699 photosynthetic traits do not change with needle age in *Pinus koraiensis* trees. New Forests 53(4):607–
700 626. https://doi.org/10.1007/s11056-021-09874-x

701 Wu H, Yin D, Salomón RL, Rodríguez-Calcerrada J, Zhang J, Zhang P, Shen H (2021) Cone-bearing
702 branches of *pinus koraiensis* are not carbon autonomous during cone development. Forests 12(9):1257.
703 https://doi.org/10.3390/F12091257/S1

Wyka and Oleksyn (2014) Photosynthetic ecophysiology of evergreen leaves in the woody angiosperms – a review. Dendrobiology 73:3–27. http://dx.doi.org/10.12657/denbio.072.001

Wyka T, Robakowski P, Zytkowiak R (2008) Leaf age as a factor in anatomical and physiological acclimative responses of *Taxus baccata* L. needles to contrasting irradiance environments. Photosynth Res 95(1):87–99. https://doi.org/10.1007/s11120-007-9238-1

Ye ZP, Robakowski P, Suggett DJ (2013) A mechanistic model for the light response of photosynthetic electron transport rate based on light harvesting properties of photosynthetic pigment molecules. Planta 237(3):837–847. https://doi.org/10.1007/s00425-012-1790-z

Yoder BJ, Ryan MG, Waring RH, et al (1994) Evidence of reduced photosynthetic rates in old trees. For Sci 40(3):513–527. https://doi.org/10.1093/forestscience/40.3.513

## Captions of tables and figures

Table 1 The photochemical parameters determined along the needle age gradient in crowns of *Abies alba*, *Taxus baccata* and *Picea abies* (means±SE, $n$ = 12). The values of Snedecor's function ($F$) and probability were obtained in one-way ANOVA (independent variable - age of needles). At the significance threshold of $\alpha = 0.05$, the distinct letters in Tukey's *a posteriori* test represent statistically significant differences between the mean values obtained for needles' various age groups. $\Phi_{PPFsat}$ - Quantum yield of PS II photochemistry at the saturation level; $PPF_{sat}$ - Quantum yield of PS II photochemistry at the saturation level of $PPF$; $ETR_{max}$ - Maximal apparent electron transport rate; $F_v/F_m$ - The maximum quantum yield of PS II photochemistry in *A. alba*, *T. baccata*, and *P. abies* needles; NAC – needle age class

Table 2 Photosynthetic pigments content along the needle age gradient in crowns of *Abies alba*, *Taxus baccata* and *Picea abies* (mean±SE, $n$ = 12). The values of Snedecor's function ($F$) together with probability were obtained in one-way ANOVA (independent variable - age of needles). At the significance threshold of $\alpha = 0.05$, the distinct letters in Tukey's *a posteriori* test represent statistically significant differences between the mean values obtained for needles' various age groups. $Chl_{tot}$ (mg $g^{-1}$) - total chlorophyll concentration (mg $g^{-1}$); $Chl_{tot}$ (g $m^{-2}$) - total needle chlorophyll content (g $m^{-2}$); $Chl_a$/ $Chl_b$ - chlorophyll *a* concentration to chlorophyll *b* concentration ratio; $Car/Chl_{tot}$ - total carotenoids to total chlorophyll ratio; NAC – needle age class

737 Fig. 1 The linear relationship between the mean relative photosynthetic photon flux (r*PPF*)
738 values and needle age classes (mean ± SE, $n$ = 12, $n$ – number of measurements per species,
739 tree and needle age class) (**a**); The relationship between the leaf mass-to-area ratio (*LMA*) *vs*.
740 needle age classes of *A*. *alba*, *T*. *baccata*, and *P*. *abies* needles (mean ± SE, $n$ = 12, $n$ - number
741 of samples per species, tree and needle age class) (**b**). In each plot, the regression equations ($y$)
742 and coefficients of determination ($R^2$) with the values of probability ($P$) are shown for each
743 species
744
745 Fig. 2 The relationship between the mean values of maximum quantum yield of PS II
746 photochemistry ($F_v/F_m$) and needle age class (**a**); The needles' age dependence of maximal
747 apparent electron transport rate ($ETR_{max}$) (**b**); Non-photochemiqal quenching of fluorescence
748 (*NPQ*) at the actinic light level of 345 μmol $m^{-2}$ $s^{-1}$ in *A*. *alba*, *T*. *baccata*, and *P*. *abies* needles
749 (mean ± SE, $n$ = 12) (**c**). In each plot, the regression equations ($y$) and coefficients of
750 determination ($R^2$) with the probability values ($P$) are shown
751
752 Fig. 3 Needles' age dependence of quantum yield of PSII photochemistry at the saturation level
753 of actinic light ($\Phi_{PFFsat}$) (**a**). The saturation level of photosynthetic photon flux ($PPF_{sat}$) in *A*.
754 *alba*, *T*. *baccata*, and *P*. *abies* needles *vs*. needle age classes (mean ± SE, $n$ = 12) (**b**). In each
755 figure, the regression equation ($y$) and coefficient of determination ($R^2$) with the probability
756 values ($P$) are shown
757
758 Fig. 4 Total chlorophyll concentration ($Chl_{tot}$, mg $g^{-1}$) (**a**); Total chlorophyll content $Chl_{tot}$ (g
759 $m^{-2}$) (**b**) in *A*. *alba*, *T*. *baccata*, and *P*. *abies* needles *vs*. the needle age classes (mean ± SE, $n$ =
760 12). In each plot, the regression equation ($y$) and coefficient of determination ($R^2$) with the
761 values of probability ($P$) are shown
762
763 Fig. 5 Total carotenoids concentration (mg $g^{-1}$) (**a**); Total carotenoids content ($gm^{-2}$) (**b**); the
764 ratio of carotenoids (mg $g^{-1}$) and total chlorophyll (**c**) in *A*. *alba*, *T*. *baccata*, and *P*. *abies* needles
765 vs. age classes of the needles (mean ± SE, $n$ = 12). In each figure, the regression equation ($y$)
766 and coefficient of determination ($R^2$) with the probability ($P$) are shown.
767
768 Fig. 6 Chlorophyll content and the ratio of chlorophyll *a* and *b* in *A*. *alba* (**a**), *T*. *baccata* (**b**),
769 and *P*. *abies* (**c**) needles *vs*. age classes of the needles (mean ± SE, $n$ = 12). In each figure, the
770 regression equation ($y$) and coefficient of determination ($R^2$) with the probability are shown.

771 Table 1

| Species | NAC | $F_v/F_m$ | $ETR_{max}$ | $\Phi_{PPFsat}$ | $PPF_{sat}$ |
|---|---|---|---|---|---|
| *Abies alba* | 1 | 0.872±0.005 | 89.44±7.91abc | 0.247±0.016 | 819.57±56.32ab |
| | 2 | 0.877±0.003 | 110.88±8.62a | 0.257±0.019 | 955.22±70.64a |
| | 3 | 0.878±0.002 | 100.23±5.19ab | 0.256±0.012 | 851.79±31.47ab |
| | 4 | 0.875±0.004 | 93.16±5.43abc | 0.252±0.007 | 793.14±39.56ab |
| | 5 | 0.879±0.003 | 87.76±5.36abc | 0.239±0.013 | 783.28±39.92ab |
| | 6 | 0.869±0.006 | 75.72±4.79bc | 0.206±0.017 | 778.64±43.73ab |
| | 7 | 0.868±0.008 | 67.29±6.08bc | 0.247±0.013 | 601.98±48.35b |
| | 8 | 0.873±0.009 | 58.06±5.73c | 0.206±0.024 | 683.56±86.99ab |
| | *F*, *P* | 0.92 | $5.60^{***}$ | 2.19 | $2.92^{**}$ |
| *Taxus baccata* | 1 | 0.857±0.006a | 79.52±6.80a | 0.193±0.020 | 964.16±139.77a |
| | 2 | 0.854±0.005ab | 77.14±6.40ab | 0.184±0.013 | 898.32±93.05a |
| | 3 | 0.844±0.004ab | 68.43±7.32ab | 0.175±0.011 | 801.51±72.88ab |
| | 4 | 0.834±0.008b | 53.66±6.05b | 0.187±0.010 | 641.20±80.19b |
| | *F*, *P* | $2.98^{**}$ | $9.14^{**}$ | 0.54 | $8.04^{**}$ |
| *Picea abies* | 1 | 0.860±0.005a | 78.62±3.60a | 0.16±0.01 | 1046.61±55.77 |
| | 2 | 0.848±0.007ab | 80.18±5.61a | 0.18±0.02 | 984.79±100.87 |
| | 3 | 0.840±0.006abc | 71.75±5.12ab | 0.18±0.01 | 853.11±61.25 |
| | 4 | 0.838±0.007abc | 71.50±4.50ab | 0.16±0.01 | 1256.5±395.34 |
| | 5 | 0.840±0.008abc | 64.01±4.89abc | 0.18±0.01 | 751.57±65.21 |
| | 6 | 0.824±0.008bc | 56.43±2.94bcd | 0.16±0.01 | 798.83±69.24 |
| | 7 | 0.825±0.008bc | 48.68±3.82cd | 0.17±0.01 | 655.88±69.98 |
| | 8 | 0.815±0.010c | 43.95±3.90d | 0.17±0.01 | 560.28±61.19 |
| | *F*, *P* | $7.49^{***}$ | $15.12^{***}$ | 0.55 | 1.38 |

772
773
774
775
776
777
778
779
780
781
782
783
784
785
786
787

Table 2

| Species | NAC | $Chl_{tot}$ (mg $g^{-1}$) | $Chl_{tot}$ (g $m^{-2}$) | *Car* (mg $g^{-1}$) | *Car* (g $m^{-2}$) | $Chl_a/Chl_b$ | $Car/Chl_{tot}$ |
|---|---|---|---|---|---|---|---|
| *Abies alba* | 1 | 3.12±0.37 | 0.94±0.14c | 0.114±0.005c | 0.0101±0.001b | 3.49±0.16ab | 0.010±0.001 |
| | 2 | 3.19±0.12 | 1.23±0.22bc | 0.134±0.005abc | 0.0123±0.001ab | 3.86±0.31a | 0.012±0.001 |
| | 3 | 3.30±0.12 | 1.62±0.31ab | 0.135±0.009abc | 0.0126±0.001ab | 3.36±0.12bc | 0.013±0.001 |
| | 4 | 2.75±0.19 | 1.88±0.42a | 0.154±0.011ab | 0.0162±0.002a | 3.29±0.16bc | 0.016±0.002 |
| | 5 | 3.42±0.53 | 1.80±0.21a | 0.156±0.009a | 0.0168±0.002a | 3.14±0.12bc | 0.017±0.002 |
| | 6 | 3.01±0.32 | 1.80±0.18a | 0.155±0.006a | 0.0138±0.001ab | 2.99±0.097c | 0.014±0.001 |
| | 7 | 3.34±0.30 | 1.65±0.22ab | 0.142±0.005ab | 0.0125±0.001ab | 3.06±0.25bc | 0.013±0.001 |
| | 8 | 3.15±0.16 | 1.46±0.27abc | 0.129±0.011bc | 0.0128±0.001ab | 2.92±0.16c | 0.013±0.001 |
| | *F*, *P* | 0.56 | $7.39^{**}$ | $8.16^{***}$ | $2.90^{**}$ | $8.98^{***}$ | 1.25 |
| *Taxus baccata* | 1 | 3.23±0.36 | 1.29±0.23 | 0.224±0.022 | 0.023±0.004 | 3.67±0.07 | 0.082±0.013 |
| | 2 | 2.62±0.26 | 2.25±0.40 | 0.216±0.027 | 0.027±0.004 | 3.42±0.22 | 0.071±0.009 |
| | 3 | 2.68±0.19 | 2.07±0.46 | 0.202±0.027 | 0.026±0.004 | 3.56±0.32 | 0.068±0.010 |
| | 4 | 3.56±0.86 | 1.64±0.36 | 0.184±0.019 | 0.020±0.004 | 3.34±0.25 | 0.051±0.008 |
| | *F*, *P* | 0.91 | 3.37 | 2.10 | 0.61 | 1.03 | 0.87 |
| *Picea abies* | 1 | 3.61±0.15 | 0.78±0.16b | 0.104±0.005c | 0.016±0.002c | 3.73±0.10a | 0.047±0.007b |
| | 2 | 2.72±0.35 | 1.76±0.4a | 0.158±0.001a | 0.032±0.002a | 3.63±0.11ab | 0.087±0.008a |
| | 3 | 2.95±0.06 | 1.48±0.25ab | 0.156±0.010a | 0.023±0.002abc | 3.24±0.03abc | 0.064±0.009ab |
| | 4 | 2.67±0.33 | 1.97±0.42a | 0.152±0.014a | 0.026±0.002ab | 3.21±0.03abc | 0.059±0.006b |
| | 5 | 2.77±0.21 | 1.7±0.28ab | 0.150±0.014ab | 0.026±0.002ab | 3.11±0.08bc | 0.069±0.008ab |
| | 6 | 2.67±0.48 | 1.60±0.36ab | 0.142±0.010ab | 0.022±0.002bc | 3.18±0.25abc | 0.063±0.007b |
| | 7 | 2.81±0.35 | 1.44±0.25ab | 0.126±0.009bc | 0.021±0.002bc | 3.06±0.05c | 0.054±0.007b |
| | 8 | 2.77±0.28 | 1.20±0.3ab | 0.108±0.006c | 0.021±0.002bc | 2.82±0.16c | 0.051±0.007b |
| | *F*, *P* | 1.35 | $3.49^{*}$ | $16.20^{***}$ | $4.82^{***}$ | $6.62^{***}$ | $6.17^{***}$ |

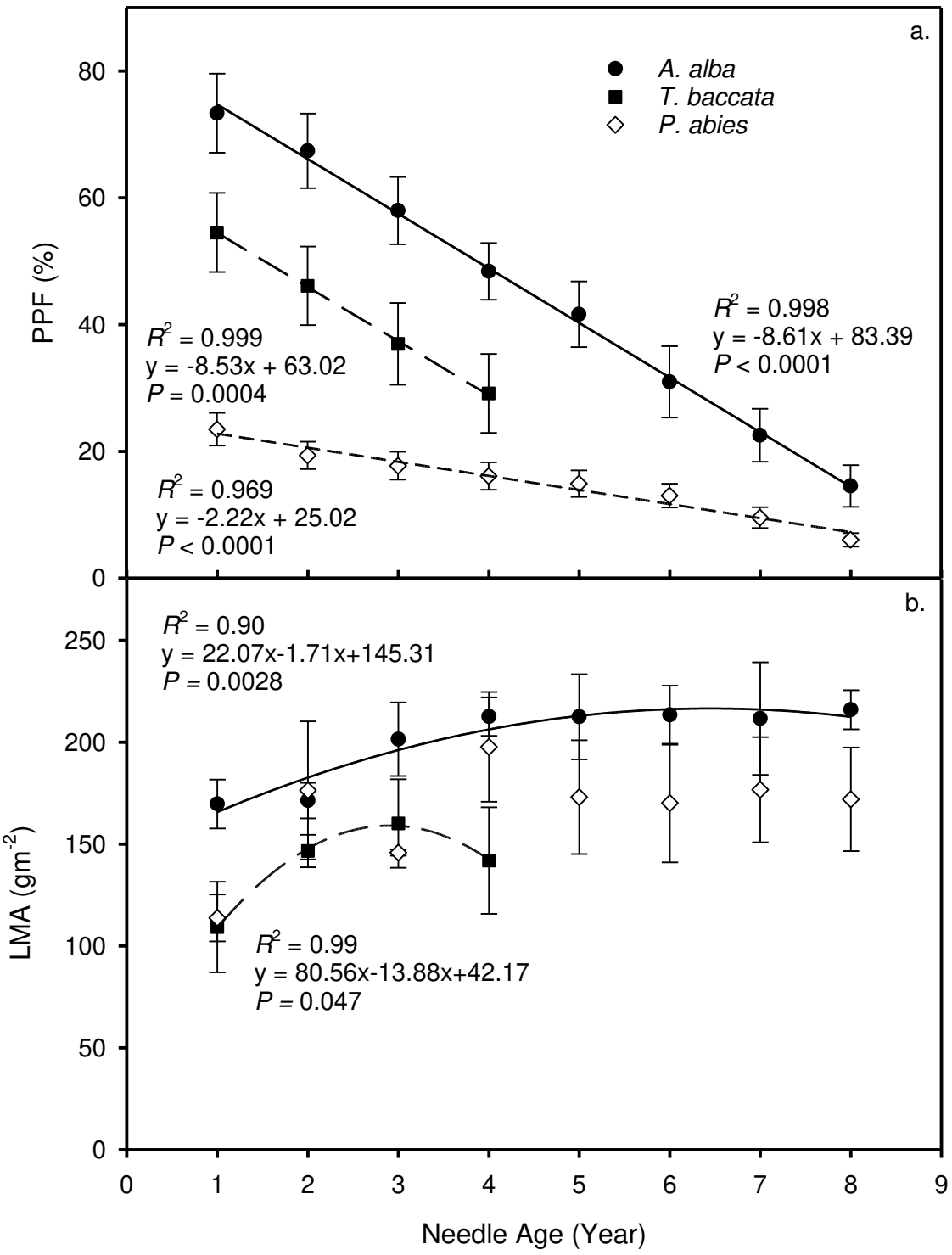


Fig. 1 sigmaplot v.13.0

800

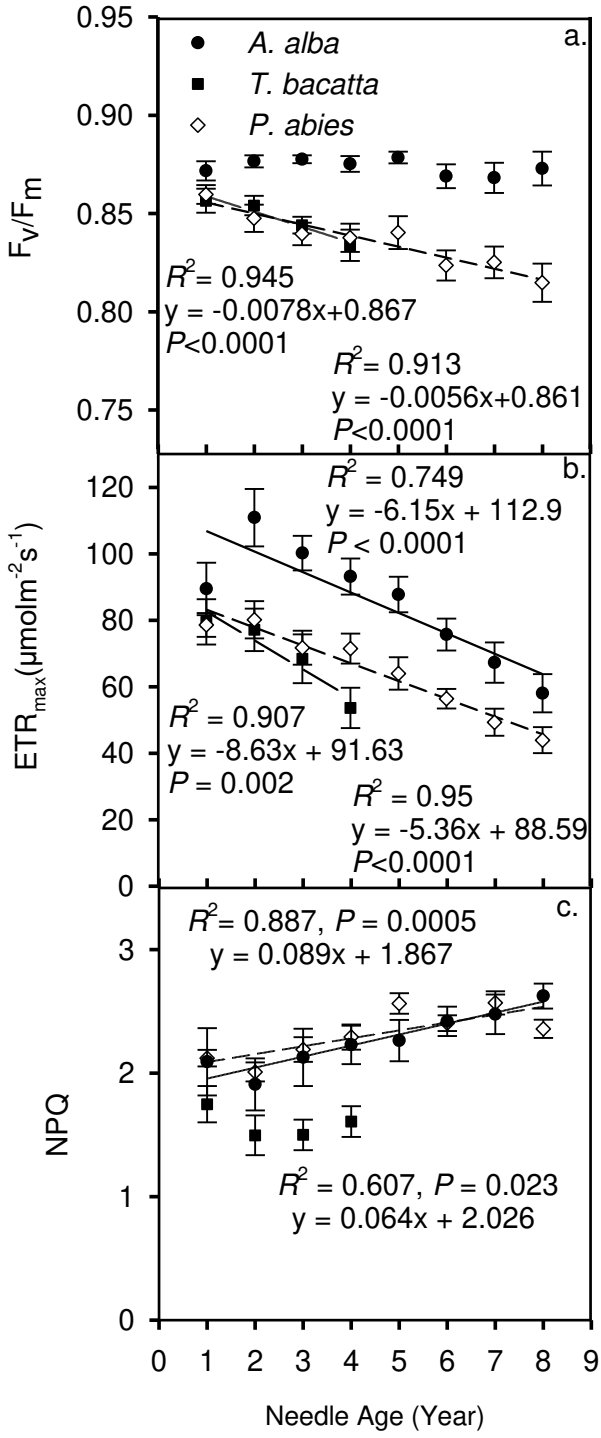


801

802 Fig. 2 sigmaplot v.13.0

803

804

805

806

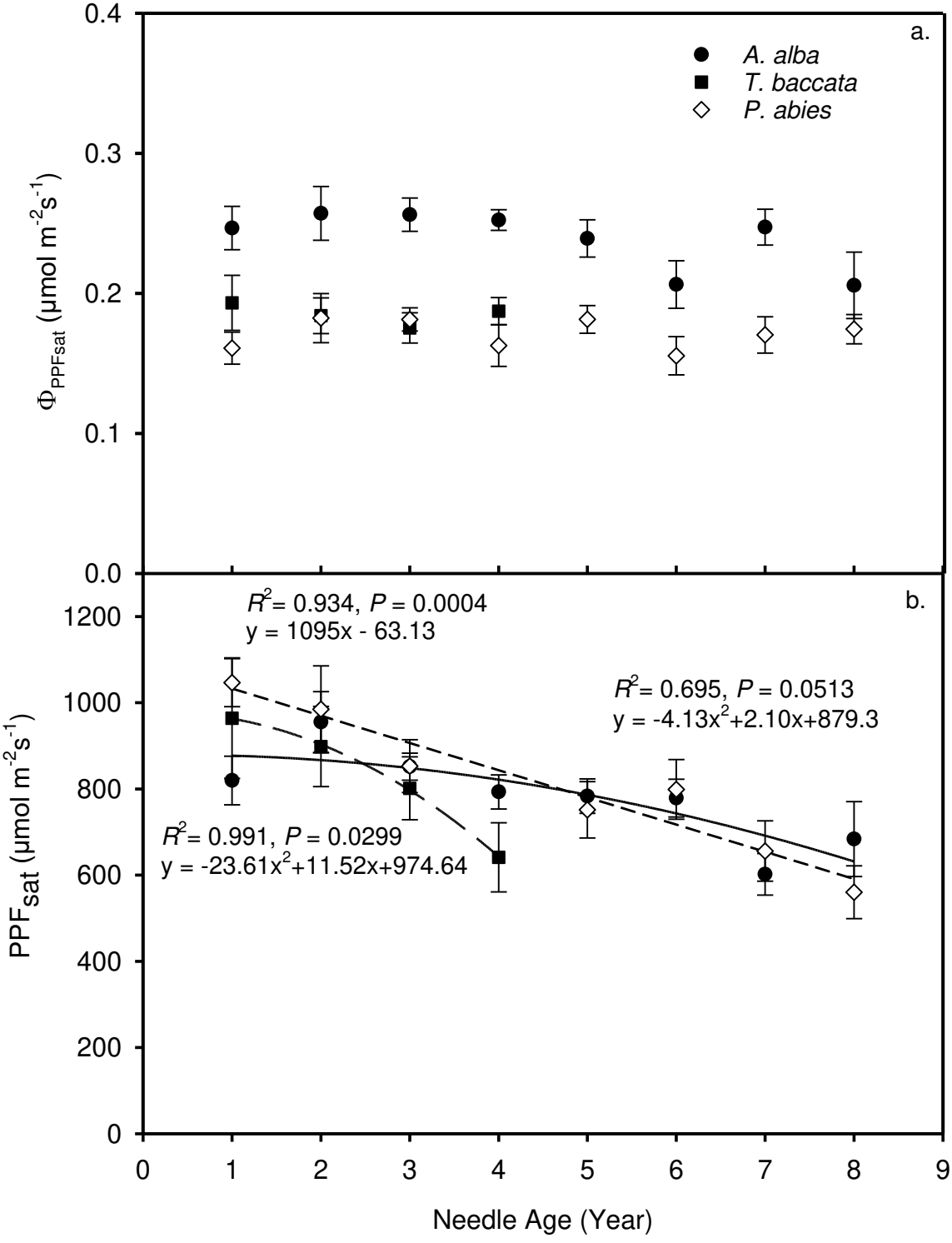


Fig. 3 sigmaplot v.13.0

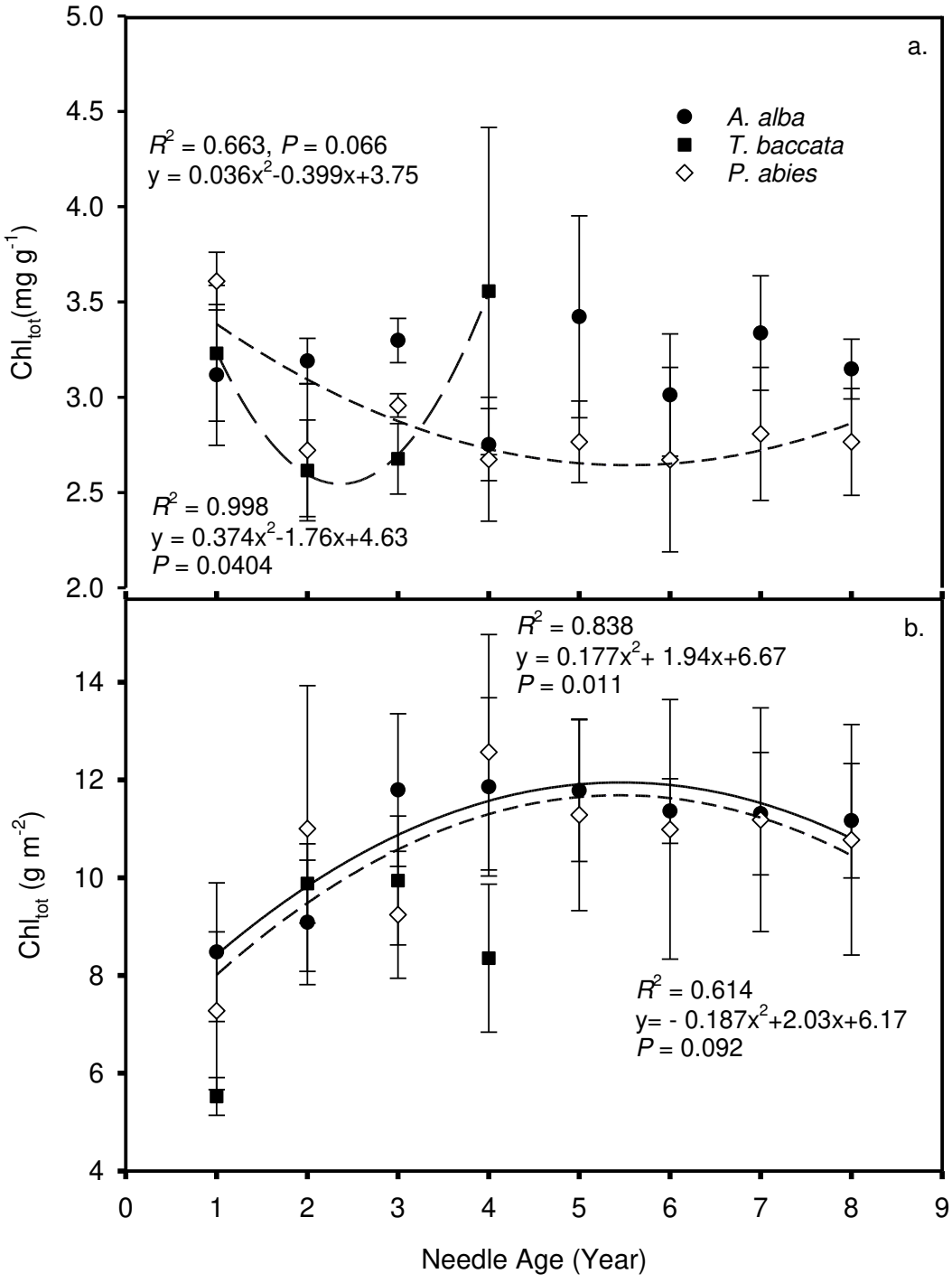


Fig. 4 sigmaplot v.13.0

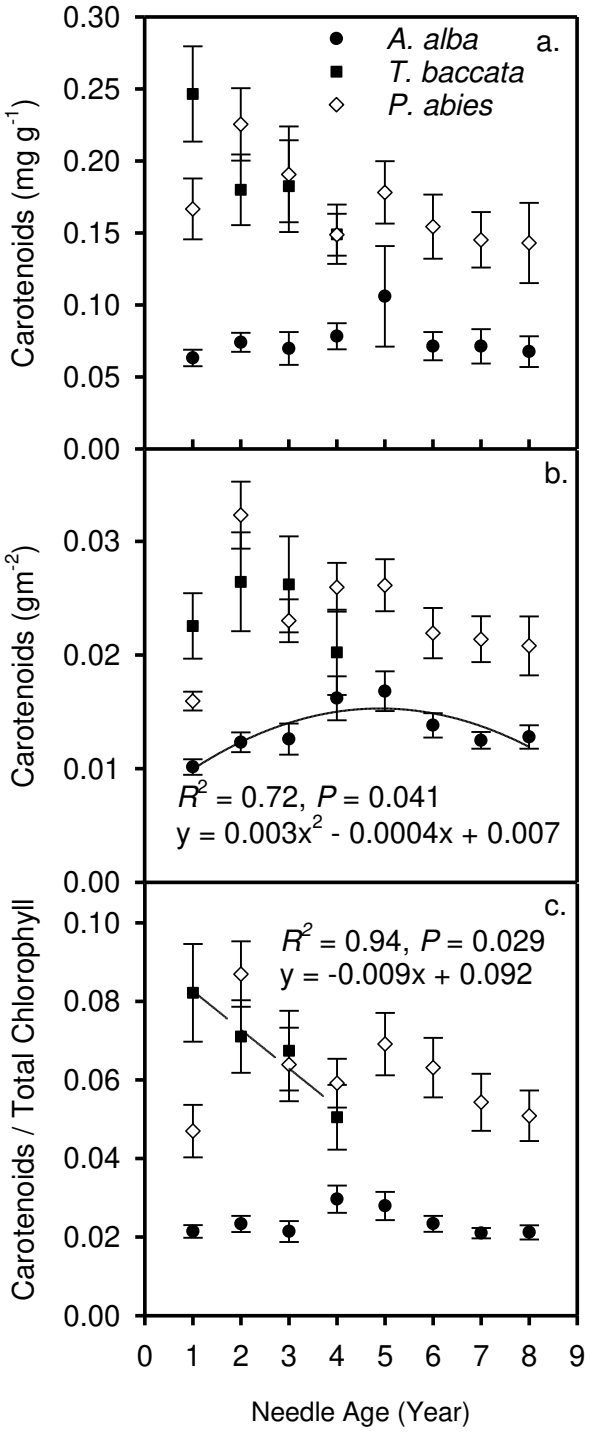


820

821 Fig. 5 sigmaplot v.13.0

822

823

824

825

826

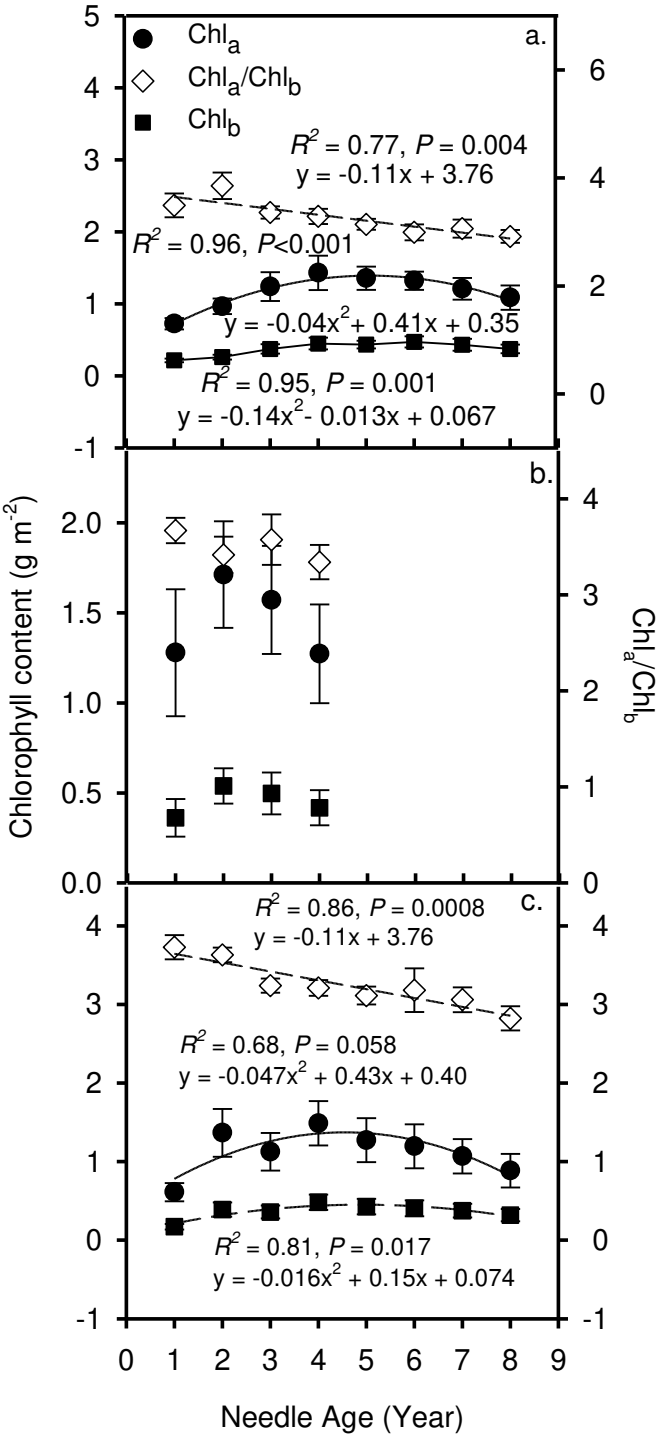


827

828

829 Fig. 6 sigmaplot v.13.0

# Supplementary Files

This is a list of supplementary files associated with this preprint. Click to download.

- Supplement.docx